CrystEngComm

PAPER

Cite this: *CrystEngComm*, 2023, **25**, 6279

Crystal engineering of a new pharmaceutical polymorph of gallic acid monohydrate: a structural comparative study and chemical computational quantum investigations†

Nasreddine Ghouari,[a] Rim Benali-Cherif, *[a] Radhwane Takouachet,[a] Wahiba Falek,[a] Djallila Missaoui,[b] Ali Rahmouni,[b] El-Eulmi Bendeif[c] and Nourredine Benali-Cherif[de]

Received 30th July 2023,
Accepted 13th September 2023

DOI: 10.1039/d3ce00766a

rsc.li/crystengcomm

Exploiting new polymorphs of active pharmaceutical ingredients (APIs) has a significant role in the development of new processes for the pharmaceutical industry. Within this context, we report in this work, the synthesis, crystal structure and Hirshfeld surface analyses and complementary computational quantum investigations of the seventh pharmaceutical polymorph of gallic acid monohydrate (GAM-VII). The structural properties have been determined from accurate single crystal data collected at 100 K and reveal that the formation and stability of this new polymorph are associated with the implementation of water molecules within the network of the moderate intermolecular interactions involving carboxyl groups. A detailed and systematic comparison of molecular conformations and packings, hydrogen bonding and intermolecular interactions of the studied polymorph (GAM-VII) was performed with the other six known GAM polymorphs. In this new polymorph, gallic acid molecules (GA) adopt *syn* COOH orientations leading to the formation of the common centrosymmetric $(COOH)_2$ dimer $R_2^2(8)$. This homo-synthon configuration was only observed in polymorphs I, III and V. Moreover, the analysis and quantification of the contributions of different intermolecular interactions within the supramolecular assemblies were conducted using the Hirshfeld surface (HS) method. This investigation allowed reflection of the offset stacking arrangement of GA molecules and the presence of $\pi\cdots\pi$ interactions between the benzene rings in the studied polymorph. Based on complementary theoretical calculations, we were able to determine and discuss many fundamental characteristics in the reactivity process of this new polymorph such as dipole moment, ionization, chemical potential, electronegativity and electrophilicity index.

Introduction

First recognized in 1822, polymorphism of crystals is now an extensively observed phenomenon. Crystal polymorphism is encountered in all fields of solid substance research and studies.[1] Polymorphism and its occurrence in fine chemicals, drugs, pharmaceuticals and other industries have been intensively studied over the last few decades.[2–5] Polymorphism of active pharmaceutical ingredients (APIs), in other words, is the ability of medications to exist in various and distinct molecular structures and differences in physico-chemical properties provoked by this phenomenon can change, such as pharmaceutical processability, bioavailability, and medication stability.[6] Pseudopolymorphism is characterized by the ability of a compound to exist in multiple crystalline forms, with variations in the stoichiometry and the nature of the solvent molecules incorporated within the crystal lattice. If the incorporated solvent is water, a solvate is termed a hydrate. Usually adducts are less difficult to combine than single molecules. Diverse hypotheses can be given, including adduct symmetry, adduct-induced conformational changes, and the ability to form hydrogen bonds through solvent molecules.[7,8]

Desiraju *et al.* have reported the possibility of using water molecules as a design element in crystal engineering.[9] Water molecules are easily inserted into a crystal structure, because of

[a] *Laboratoire des Structures, Propriétés et Interactions Interatomiques, Université Abbes Laghrour-Khenchela, 40000 Khenchela, Algeria.*
E-mail: benalicherif.rim@univ-khenchela.dz
[b] *Laboratoire de Modélisation et de Méthodes de Calcul, University of Saida Dr. Moulay Tahar, Saida, Algeria*
[c] *Université de Lorraine, CNRS, CRM2, 54000 Nancy, France*
[d] *Académie Algérienne des Sciences et de la Technologie (AAST) Algiers, Algeria*
[e] *Mohamed Seddik Ben Yahia University, 18000 Jijel, Algeria*

† Electronic supplementary information (ESI) available. CCDC 1533012. For ESI and crystallographic data in CIF or other electronic format see DOI: https://doi.org/10.1039/d3ce00766a

their small size, flexibility of placement, excellent interaction ability and multidirectional hydrogen bonding capacity. The role of water molecules in the solid-state chemistry of active pharmaceutical ingredients (APIs) is remarkable.[3,10] Many drug molecules are large and malleable; they encompass a variety of hydrogen bond donors and acceptors. They are, therefore, particularly prone to hydration. Approximately 1/3 of pharmaceutical molecules are thought to be capable of forming hydrates in crystalline forms.[11] A Cambridge Structural Database (CSD)[12] survey reports that among the 1 247 617 deposited crystal structures, 154 663 (~12.4%) are hydrated. Several studies have been published exploring the interactions of water molecules in crystalline hydrates with the active pharmaceutical ingredient (API).[13] Additionally, APIs are susceptible to forming hydrates, and hydrates are sometimes the preferred crystalline form for drug delivery.[14] Gallic acid (GA) (3,4,5-trihydroxybenzoic acid) is one of the abundant, therapeutic and bioactive phenolic compounds found in *Choerospondiatis fructus*, a Mongolian medicinal plant, used to treat some diseases, particularly myocardial infarction and angina pectoris.[15] Gallic acid is an active pharmaceutical element (API) containing two of the most omnipresent functional groups of APIs: phenols and carboxylic acids. According to the US FDA gallic acid is a GRAS molecule that exhibits anticholesterol, antitubercular, antifungal, antibacterial, antiviral, anti-obesity, anti-ulcer, and immunomodulatory activities.[16–18] It also displays antimicrobial, anticancer and antioxidant properties.[19] Gallic acid has three hydroxyl groups which can act as both donors and acceptors of hydrogen bonds. The O–H carboxy hydrogen atom has a strong hydrogen bonding donor property and the C═O moiety of the acid function has a strong hydrogen bonding acceptor property. Moreover, GA has many possible conformers depending on the orientations of its three OH and COOH groups; some were studied by spectroscopic and theoretical methods.[20] Thus, all the characteristics and properties of GA allow it to exhibit polymorphism and pseudo-polymorphism.[21] The prediction of forms III and IV of gallic acid monohydrate (GAM) in the fifth blind test for the Crystal Structure Prediction (CSP2010) was given as a challenge for the first time to predict the structures of additional and unpublished polymorphs of a hydrate given that two polymorphs, forms I and II,[22,23] were already in the Cambridge Structural Database.[12] Afterwards, the target structures were published exhibiting outstanding hydrate polymorphism.[24,25] Braun *et al.*[26] reported in their study the structure of five monohydrates of GA and two additional anhydrate polymorphs and at least 22 other solvates formed. They showed in their survey that the crystal energy landscapes for anhydrous and monohydrate forms of GA that have various packing motifs and hydrogen bonding are highly competitive in energy and exhibit numerous thermodynamically feasible structures, which explains why GA shows this remarkable tendency toward polymorphism. In 2017, the sixth polymorph of gallic acid monohydrate was observed at 10 K by Hoser *et al.*[27] Further, anhydrous gallic acid is also polymorphic, three hydrate-free

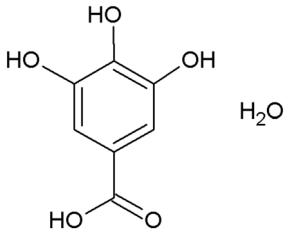

Scheme 1 Gallic acid monohydrate.

structures have been published[26,28] and their structures were deposited in the CSD. Each gallic acid monohydrate polymorph has a different arrangement and conformation due to the distinct synthons and various intra/intermolecular hydrogen bonds of GA with water molecules. As part of our team's efforts to investigate original polymorphs, we chose to work on compounds rich in hydrogen bonds based on acids, amines and nitrogen bases.[29,30] Still, it is not always easy to obtain a particular polymorph under controlled conditions. During the last few years, we have succeeded in synthesizing new polymorphs by acting on crystallization conditions.[31,32] In this paper, GA is used because of its richness in hydrogen bonds and the several possibilities of hydroxyl group orientation. It is also unique in the diversity shown by exhibiting polymorphism in its hydrated or anhydrous forms. In the present study, the low-temperature structural properties of the seventh polymorph of GAM (Scheme 1) are discussed and compared with those of the six polymorphs reported previously. Further, Hirshfeld surface analysis was extensively carried out for the seven polymorphs to understand the various intermolecular interactions. Moreover, to learn more about the stacking modes' effect on the molecular properties of GAM polymorphs, we employed computational quantum chemistry approaches. Computational chemistry is the study of problems based on quantum and non-quantum mechanical calculations. It numerically provides important data on the chemical structures and reactions applying fundamental laws of physics. Several factors of the GA electronic density must be known to understand the stacking effects. These global electronic descriptors give an idea about a molecule's sensitivity to structural perturbations and responses to changes in the external environment. We will discuss in this work the following global descriptors: dipole moment, ionization potential, vertical electron affinity, chemical potential, electronegativity, hardness, softness and electrophilicity index. These quantities were calculated according to the approach defined by Rajan and Muraleedharan.[33]

Experimental section

Synthesis and crystallization of the GAM-VII polymorph

Gallic acid monohydrate was purchased from BIOCHEM and used without any further purification. In a stoichiometric ratio, gallic acid (0.40 g, 0.0024 mol) was dissolved in hot (~338 K) distilled water (approximately 30 ml). The obtained mixture was stirred on a hot plate with slow evaporation for

30 min. The solution was left at room temperature for crystallization by very slow evaporation and after three weeks brown plate single crystals appeared. The selected single crystals of GAM-VII were subjected to X-ray diffraction analysis.

Single crystal X-ray diffraction and structure refinement details

Single crystal diffraction measurements were performed on a Rigaku SuperNova diffractometer with graphite monochromatized Mo K_α radiation, λ = 0.71073 Å. The main crystallographic data, measurements and structure refinement details of GAM-VII are summarized in Table 1. The structure was solved by direct methods using the program SIR2014 (ref. 34) and was refined against F^2 by weighted full-matrix least squares methods including all reflections with the SHELXL-2018 program.[35] All calculations were carried out using the WingX software package.[36] To take into consideration the disorder of the water molecule O2W manifested by abnormally high atomic displacement parameters (ADP), we split the position of the oxygen atom (O2W) along the longest ADP axis into two groups (Part 1: O2WA and Part 2: O2WB) and link their complementary occupancy (0.541 and 0.459 for Part 1 and Part 2 respectively) through a free variable. Structural representations were drawn using MERCURY.[37] All non-H atoms were refined anisotropically, and all hydrogen atoms were located in difference density Fourier maps.

Table 1 Main crystallographic data and structure refinement details for GAM-VII

Crystal data	
Chemical formula	$2(C_7H_6O_5)$, $2(H_2O)$
M_r	376.27
Crystal system, space group	Triclinic, $P\bar{1}$
Temperature (K)	100 (2)
a, b, c (Å)	7.1034(6), 7.4941(6), 15.5567(12)
α, β, γ (°)	100.593(3), 91.274(3), 111.564(3)
V (Å^3)	753.39(11)
Z	4
Radiation type	Mo Kα
μ (mm^{-1})	0.15
Crystal size (mm)	0.140 × 0.120 × 0.105
Data collection	
Diffractometer	SuperNova, Dual, Cu at zero, Atlas Diffractometer
No. of measured, independent and observed [$I > 2\sigma(I)$] reflections	51 111, 8115, 6392
R_{int}	0.057
Refinement	
$R[F^2 > 2\sigma(F^2)]$, w$R(F^2)$, S	0.058, 0.154, 1.15
No. of reflections	8115
No. of parameters	234
H-atom treatment	All H-atom parameters refined
$\Delta\rho_{max}$, $\Delta\rho_{min}$ (e Å^{-3})	0.80, −0.44

Calculations details

All chemical quantum calculations were performed on experimental GA geometries at the Moller Plesset post Hartree–Fock level of theory. The correlation energy was included at the second correction level of perturbation theory MP2. All atomic orbitals were represented using the aug-cc-pvdz basis set. All the computational works were performed using the Gaussian 09 package.[38] Gaussian input files were prepared, and the output ones were analyzed using the Gaussview package.

Results and discussion

Structural description

Based on the internal arrangement and orientation of the different OH groups, GA exhibits a very rich polymorphism. If we take as a reference the OH group of the acid function, we can consider obtaining eight (08) different polymorphs (Scheme 2) which we will name according to their orientation as follows:

M_1: OH in the *meta* position and on the same orientation of the OH acid.

$\bar{M}_1$: OH in the *meta* position and on the opposite orientation of the OH acid.

M_2: OH in the *meta* position and on the same orientation of the OH acid.

$\bar{M}_2$: OH in the *meta* position and in the opposite direction of the OH acid.

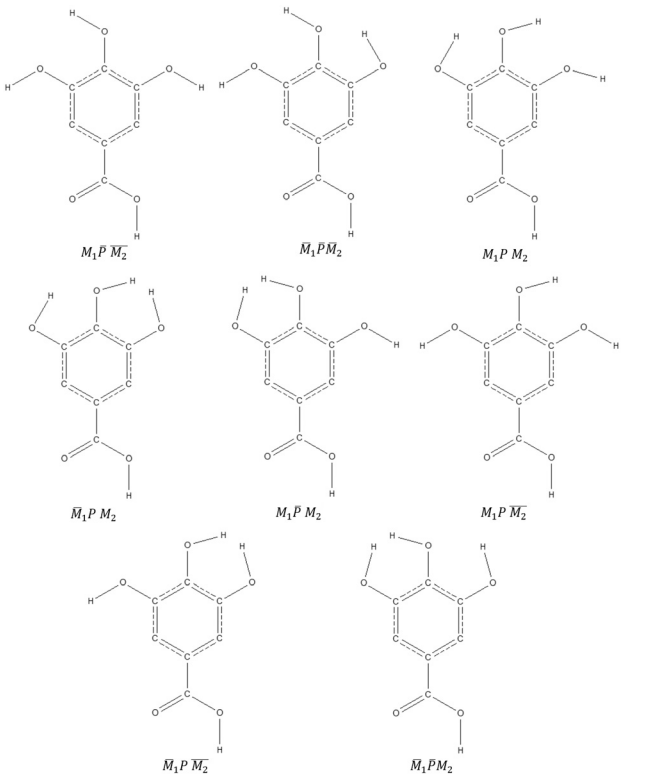

Scheme 2 The different possible orientations of hydroxyl groups in GA.

P: OH in the *para* position and on the same orientation of the OH acid.

$\bar{P}$: OH in the *para* position and in the opposite direction of the OH acid.

These different polymorphs are therefore derived from the conformational changes of the OH groups. These changes can be induced either by the crystallization methods and conditions or by solvents and polar entities present in the crystallization solutions. At the molecular packing level, these changes result in a significant difference in the number and structure of intra and intermolecular interactions as well as in the geometrical aspects of the O–H···O hydrogen bonds.

Eighty-five structures (85) of co-crystals based on gallic acid are listed in the CSD.[12] Among them are eight (08) hits of GA molecules classified in three (03) polymorphs of GA crystallizing in the anhydrous state, with the following Refcodes: IJUMEG,[28] IJUMEG04,[26] and IJUMEG06.[26] These three polymorphs adopt either the $\bar{M}_1\bar{P}\bar{M}_2$ orientation or M_1PM_2 orientation.

The crystallization of GA in the hydrate form gave rise to seven (07) polymorphs of gallic acid monohydrate (Table S1†). The presence of water molecules in the crystalline stack conferred to the different phenol group conformations and orientations of the GA molecule (Table S1†).

The crystal structure of the new polymorph of gallic acid monohydrate GAM-VII belongs to the triclinic $P\bar{1}$ space group. The asymmetric unit (Fig. 1) consists of two structurally independent molecules (A and B) of gallic acid and two water molecules one of which presents a disorder. One can clearly observe that two hydrogen atoms of two hydroxyl groups in the two GA molecules are in reverse orientation to the remaining OH atom.

The geometrical parameters are in agreement with previously reported results.[22,27] The aromatic C–C bond lengths range from 1.381(2) to 1.404(2) Å, with average values of 1.395(2) and 1.394(1) Å for molecules A and B respectively. However, the molecular structure shows a disorder of the O2W water molecule. This disorder of the water molecule has not been observed in any other polymorph of GAM.

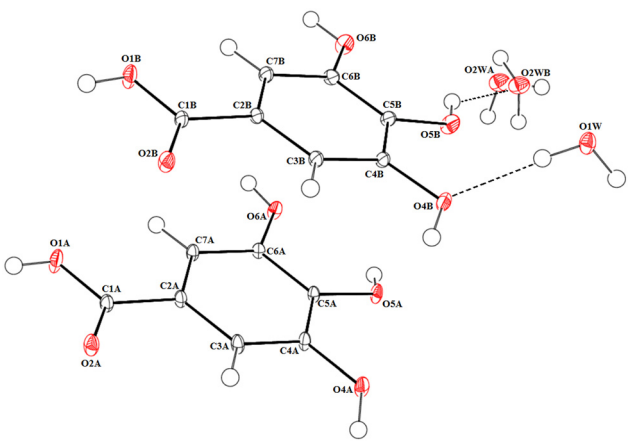

Fig. 1 The asymmetric unit of GA-VII with displacement ellipsoids shown at the 50% probability level. One of the two water molecules is disordered.

The crystal packing consists of pairs of GA molecules (A with B) linked together in a head-to-head fashion to form typical carboxylic acid $(GA)_2$ dimers, *via* moderately strong O–H···O hydrogen bonds [O1B–H1B···O2A^{vi} and O1A–H1A···O2B^{vi}], thus generating an $R_2^2(8)$ homosynthon motif[39] as shown in Fig. 2b.

The extremity of each dimer is linked on one side directly to another dimer *via* three O···O electrostatic interactions, thereby generating two heterosynthons. The other side is connected to another dimer through two O1W water molecules *via* four O–$H_{(water)}$···$O_{(ph)}$ hydrogen bonds, giving rise to an $R_4^4(14)$ tetrameric motif. These connections give rise to a zigzag 1D chain along the crystallographic *c*-axis (Fig. 2b). These 1D chains are connected to each other *via* four water molecules and two C–H···O and two O–$H_{(ph)}$···O=$COH_{(acid)}$ hydrogen bonds. In addition, the combination between these chains by means of intermolecular interactions produces five different graph-set motifs denoted as $R_3^2(11)$, $R_4^2(18)$, $R_4^2(10)$, $R_2^2(7)$ and $R_3^2(11)$ which are clearly depicted in Fig. 2b.

Moreover, GA pairs are arranged together into one-dimensional ribbons along the *b*-axis, where the ribbon edges are framed by water molecules. Each ribbon is made up of dimers formed by the association of molecules A and B. These tapes stack together to form parallel sheets along the crystallographic *a*-axis (Fig. 2a and b). This stacking has already been observed in polymorph-III of GAM (Fig. 4).[24]

Further, water molecules play an essential role in the three-dimensional network of GAM-VII. Indeed, O1W and O2W water molecules contribute to bridging the two: one-dimensional ribbons and three successive sheets *via* hydrogen bond interactions (Fig. 2a and Table 2). The O1W water molecule exhibits dual functionality, acting as a double hydrogen-bond acceptor and as a double hydrogen-bond donor, while the disordered O2W water molecule is a triple donor and double acceptor of hydrogen bonds.

Besides these hydrogen bonds, the crystal packing of GAM-VII is also characterized by $O_{(acid)}$···$C_{(acid)}$, $C_{(ring)}$···$C_{(acid)}$ and $O_{(ph)}$···$C_{(ring)}$ inter-layer electrostatic contacts. Moreover, the OH phenol oxygen atom O6A exhibits an electrostatic contact with the π-hole of the C4B carbon atom of the benzene ring, resulting in a short O6A···$C4B_{ring}$ contact, and the distance of O6A to the ring plane is only 3.168(2) A°. This $C_{(ring)}$···$O^{\delta-}$ supramolecular association contributes to the stabilization of the molecular structure of GAM-VII (Fig. 3). The $O_{(ph)}$···$C_{(ring)}$ interlayer contacts have not been observed in any other polymorph of GAM. Additionally, the stacking is also characterized by the presence of π···π non-covalent interactions, which are associated with π-hole–(C)···π-hole–(C) contacts, allowing the formation of a highly linked three-dimensional network of intermolecular interactions.

Each GA dimer forms twelve aromatic stacking interactions, *i.e.* six on one side of the fragment and six on the other. The same behaviour has also been observed in polymorph-V.[26]

In form V,[26] the absence of $O_{(acid)}$···$C_{(acid)}$ contacts has been ascertained, while concurrently, the existence of $C_{(acid)}$···π-hole electrostatic interactions has been identified in both forms III and V. This electrostatic contact concerns the interaction

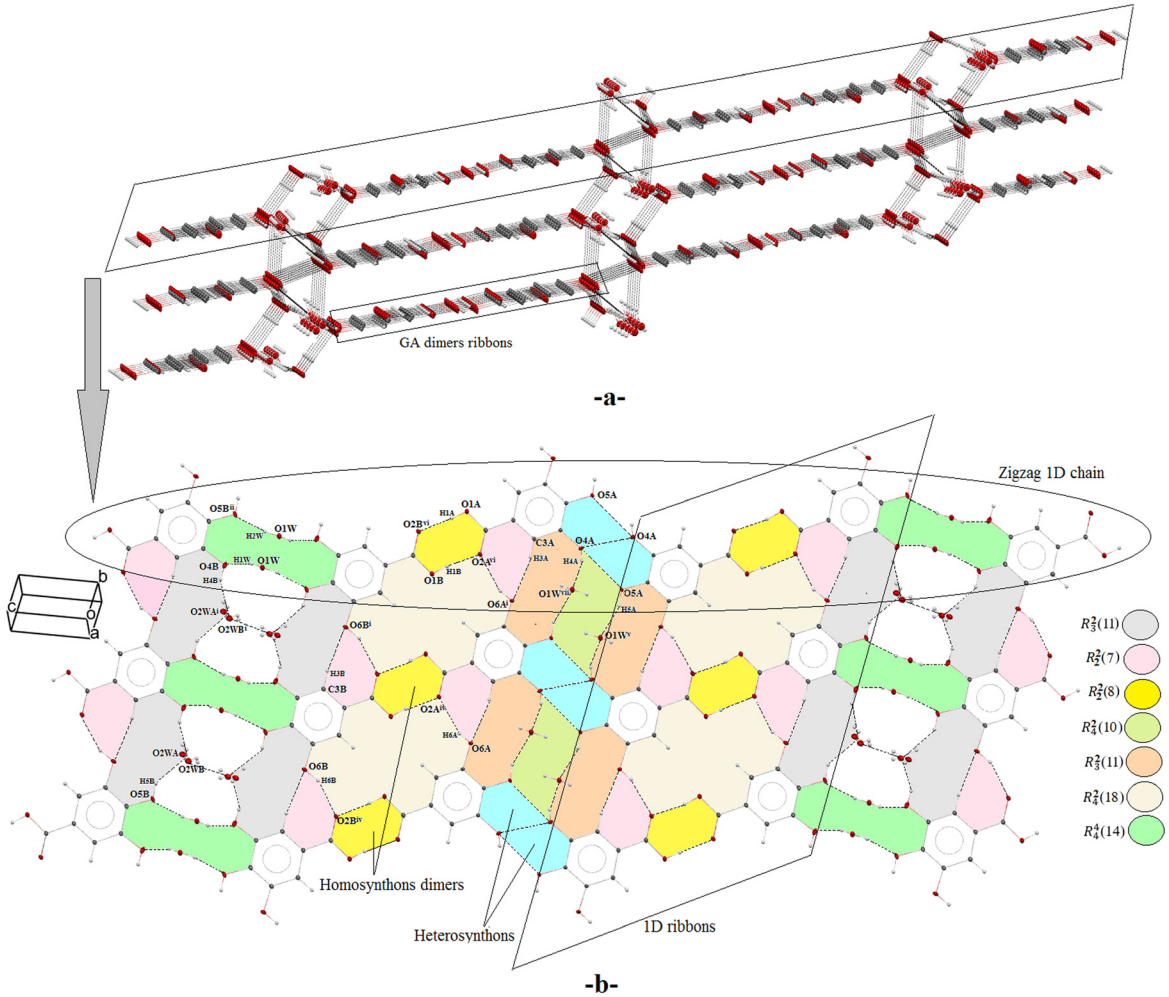

Fig. 2 (a) The crystal packing of GAM-VII in projection along the *b*-axis. For clarity, electrostatic interactions between layers have been removed. (b) A fragment of GAM-VII showing the 1D GA dimer ribbons, the supramolecular synthons and the graph set describing intermolecular interactions.

involving the $C_{(acid)}$ atom and the π-hole of the aromatic carbon atoms, resulting in a $C_{(acid)}\cdots C_{(ring)}$ contact. Moreover, apart from π⋯π interactions, no additional stacking contacts have been observed in polymorphs II[23] and IV.[24] Further, no electrostatic interaction was observed between aromatic rings in polymorph-I[22] due to the long centroid–centroid distance with a value of 5.794 Å.

Polymorphs I, III, V and VII (Fig. 3 and 4) of GAM are characterized by the presence of a centrosymmetric homosynthon dimer leading to the formation of $R_2^2(8)$ ring motifs through a double O–H⋯O interaction involving the carboxylic acid groups. These dimers are linked into sheets through $O–H_{(ph)/(water)}\cdots O_{(ph)/(water)}$ hydrogen bonding.

In polymorph-I, GA molecules form two distinct layers (Fig. 4) that build sheets developing in two different orientations (110) and ($\bar{1}$10). These two types of sheets are arranged perpendicularly and interact through $O–H_{(ph)/(water)}\cdots O_{(ph)/(water)}$ hydrogen bonds, forming a different 3D interpenetrated network. This perpendicular arrangement has been observed in one of the anhydrous forms of gallic acid.[26]

In polymorphs III and VII the sheets formed are growing parallel to the same *a*-axis, whereas in polymorph-V the sheets are deployed in a zigzag pattern along the crystallographic *c*-axis. The three structures are built up from tunnels, prolonged along the *b*-axis for III and VII polymorphs and along the *a*-axis for V polymorph (Fig. 4).

In polymorphs II, IV and VI, GA and water molecules form linear tapes *via* $OHC{=}O_{(acid)}\cdots water\cdots OH_{(ph)}$ hydrogen bonds. These tapes are in turn connected *via* supramolecular homo and hetero synthons to afford corrugated sheets in polymorph-II and to form a herringbone pattern in polymorphs IV and VI. It is interesting to note that polymorphs II and IV contain channels running through the *c* and *a*-axis respectively (Fig. 4).

Hirshfeld surface analysis

Understanding and analysing intermolecular interactions in crystal packing is essential to design new materials with desirable physical and chemical properties. Within the structures, contact types were computed by Hirshfeld surface

Table 2 Hydrogen-bond geometry (Å, °) for GAM-VII

D–H···A	D–H	H···A	D···A	D–H···A
O4B–H4B···O2WA^{i}	0.823(8)	1.743(8)	2.522(1)	158.74(8)
O4B–H4B···O2WB^{i}	0.822(8)	2.013(9)	2.737(1)	148.22(9)
C3B–H3B···O6B^{i}	0.935(8)	2.477(9)	3.373(1)	163.40(7)
C3A–H3A···O6A^{i}	0.933(8)	2.466(9)	3.368(1)	165.30(6)
O1W–H1W···O4B	0.857(9)	1.908(9)	2.723(1)	163.05(9)
O1W–H2W···O5B^{ii}	0.857(9)	1.997(8)	2.828(1)	169.53(8)
O2WA–H1WA···O5A^{iii}	0.854(8)	2.376(8)	3.005(2)	132.89(7)
O2WA–H1WA···O4A^{iv}	0.852(8)	2.101(8)	2.842(2)	146.88(6)
O2WB–H2WB···O5A^{iii}	0.855(8)	2.122(8)	2.938(2)	162.74(6)
O2WB–H2WB···O4A^{iv}	0.854(9)	2.632(8)	3.175(2)	123.04(8)
O2WB–H1WB···O4B^{iv}	0.851(9)	1.944(8)	2.738(2)	156.50(6)
O5A–H5A···O1W^{v}	0.8134(8)	1.977(9)	2.733(1)	155.44(6)
O6B–H6B···O2B^{iv}	0.8596(9)	2.0357(8)	2.839(1)	155.24(6)
O6A–H6A···O2A^{iv}	0.7730(8)	2.1211(8)	2.860(1)	160.19(6)
O1B–H1B···O2A^{vi}	0.8542(8)	1.7852(8)	2.635(1)	172.93(6)
O1A–H1A···O2B^{vi}	0.8213(8)	1.8059(8)	2.627(1)	179.04(7)
O4A–H4A···O1W^{vii}	0.7905(8)	1.9345(9)	2.695(1)	162.22(7)
O5B–H5B···O2WA	0.8052(9)	1.9508(1)	2.665(1)	147.39(8)
O5B–H5B···O2WB	0.8052(9)	1.990(1)	2.639(1)	136.55(8)

Symmetry codes: (i) $x, y-1, z$; (ii) $-x+1, -y+1, -z+1$; (iii) $-x, -y+1, -z+1$; (iv) $x, y+1, z$; (v) $x-1, y, z$; (vi) $-x, -y, -z+2$; (vii) $x-1, y-1, z$.

analysis using CrystalExplorer software[40] in order to highlight which contacts play a major role in the crystal packing stabilization. Each molecule in the asymmetric unit of a given crystal structure has a unique Hirshfeld surface. As the molecular environment directly influences the Hirshfeld surface, the area volume and the number of HS in a given crystal structure depend on the number of molecules in the corresponding asymmetric unit and the intra-asymmetric unit interactions that connect them. For example for structures with $Z > 1$, the number of unique Hirshfeld surfaces is greater than one. Therefore, the number of molecules in the asymmetric unit directly affects the volume occupied by the Hirshfeld surface, and this explains the difference between the d_{norm} representations of the seven polymorphs (Fig. 5). The fingerprint plot was devised to represent in a 2D format the mapping of d_i and d_e, which are the distances from the Hirshfeld surface to the nearest atoms inside and outside the surface, respectively. Two different but potentially useful distance measures on a 3D molecular surface, using Hirshfeld surface analysis of the seven polymorphs of GAM, were studied to clarify the nature of intermolecular contacts and are depicted in Fig. 5. The information regarding intermolecular contacts of GAM-VII presented in Table 2 is summarized effectively in the spots of the Hirshfeld surface mapped over d_{norm} (Fig. 5). Indeed, for the seven polymorphs, the deep red spots present near the water molecules, phenol and acid groups indicate the close-contact interactions, which are mainly responsible for the significant intermolecular O–H···O hydrogen bonds. The light-red spots on Hirshfeld surfaces indicate the C–H···O interactions, whereas the white spots on the surfaces indicate longer and weaker contacts other than hydrogen bonds. Not only hydrogen bonding interactions can be explored by HS analysis but also comparatively weak interactions involving phenyl rings can be explored. Fig. 5 presents Hirshfeld surfaces mapped with d_{norm} and 2D fingerprint plots for the seven polymorphs of GAM. This shows the Hirshfeld surfaces of all GAM polymorphs as part of their molecular-packing arrangements. An imprint due to the adjacent aromatic ring is visible on the d_e surfaces, which appear as a deep blue spot on the d_e surface (indicated by arrows in Fig. 5), reflecting the offset stacking arrangement in the crystal. These spots are shifted from the aromatic ring centers, thereby providing further evidence to the different offsets in π···π aromatic stacking in GAM polymorphs.

In the packing layers, the largest shift of GA molecules with the molecules below and above the plane is observed for polymorph-I; this can be explained by the results obtained by X-ray diffraction, showing an inter-centroid separation of 5.794(6) Å (Fig. 3). This long inter-centroid distance may also explain the absence of π···π interactions in polymorph-I.

In the shape index representations, the pattern of red and blue triangles on the index surface (the bicolour triangle pairs surrounded by the black circles in Fig. 5) is another characteristic of π···π interactions. Blue triangles represent convex regions due to ring carbon atoms of the molecule inside the surface, while red triangles represent concave regions due to carbon atoms of the π-stacked molecule above it. The pattern of alternating red and blue triangles is indicative of offset π···π stacking interaction characteristic. These π···π contacts are present in polymorphs II, III, IV, V, VI and VII but not in polymorph-I. Fingerprint plots for the seven polymorphs of GAM are shown in Fig. 5. All these fingerprint plots show a prominent pair of light green colour spikes with diffuse regions of points in between; for I, III, V and VII polymorphs these pairs are the pattern characteristic of a cyclic $R_2^2(8)$ hydrogen-bonding motif. On the other hand, for polymorphs II, IV and VI which do not form a typical carboxylic acid dimer, these two long

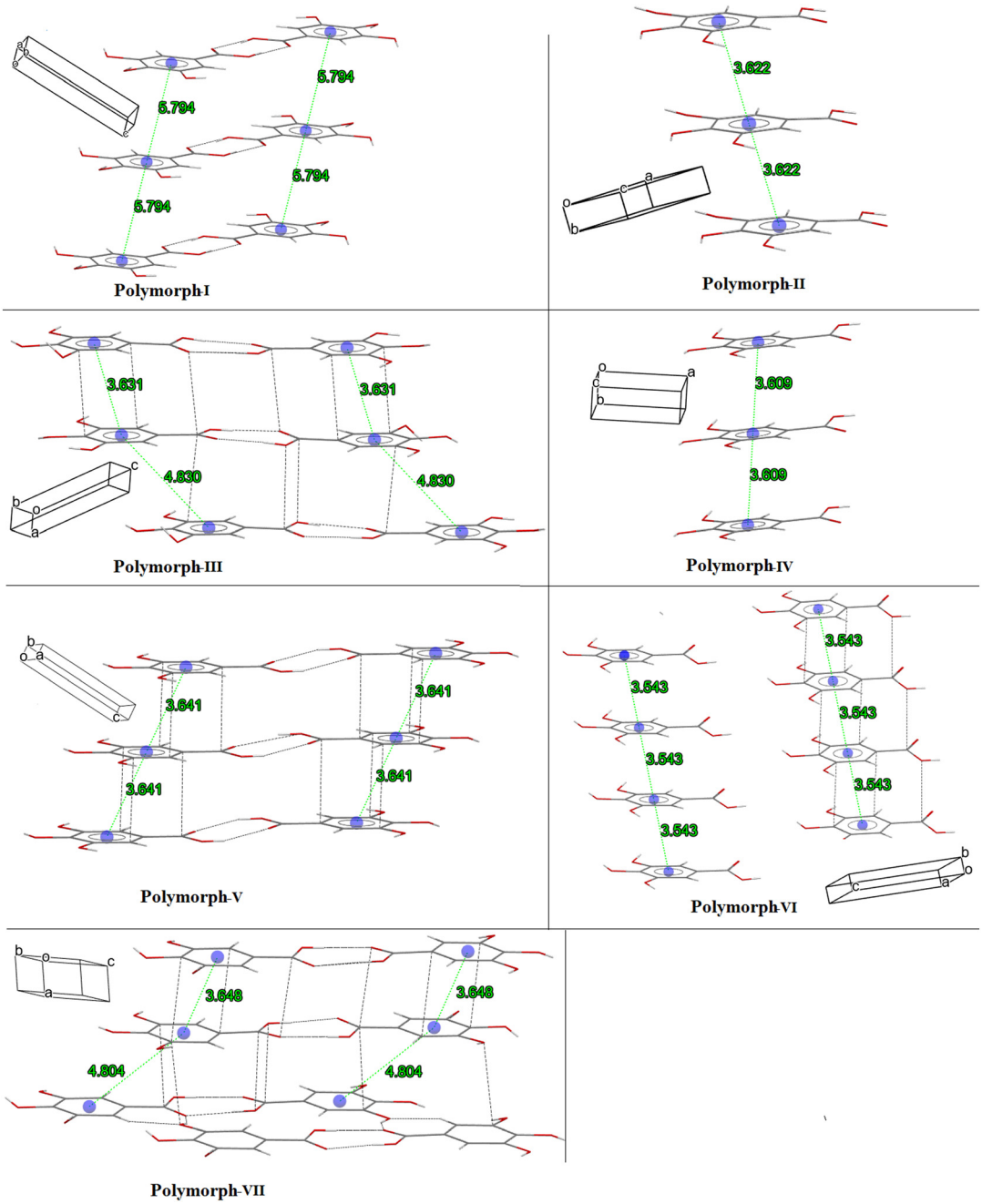

Fig. 3 The molecular packing of the seven polymorphs of GAM, showing distances between centroids and electrostatic interactions (black dotted lines) between GA molecules. The distances are measured in Å.

spikes are characteristic of $O–H_{acid}\cdots O_{water}$ interactions. Further, in polymorph-VII, between the two prominent green spikes, there exist two additional elongated blue peaks, hitherto unobserved in all other polymorphs of GAM. These spikes are attributed to interactions between the $OH_{(ph)}$ with the disordered water molecule.

Computational quantum chemistry results

Table 3 shows the calculated relative energies and global electronic density descriptors of GA structures within GA monohydrate polymorphs. Based on relative energy calculations, it can be inferred that the most stable structure is polymorph V. Indeed, the most stable polymorph typically corresponds to the one with the lowest relative energy. Relative energy takes into account the interactions between atoms and the crystal structures, providing a theoretical perspective on the stability of polymorphs.

In the study of polymorphism and intermolecular interactions, dipole moment calculations play a crucial role in quantifying the polarity of molecules and crystals, providing insights into the nature and strength of polar

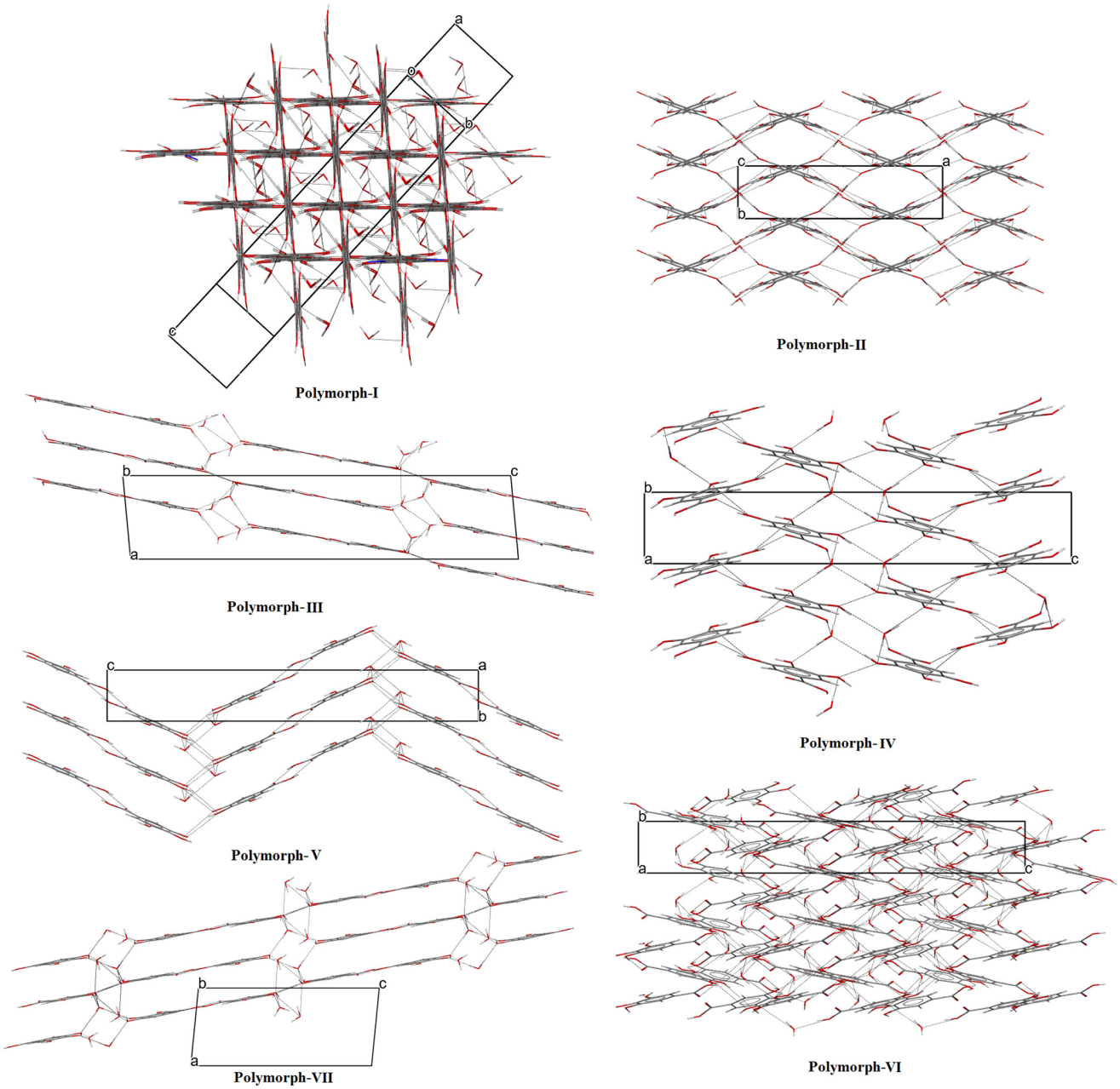

Fig. 4 Crystal packing of GAM polymorphs I, II, III, IV, V, VI and VII. The left side indicates polymorphs that form dimers, and the right side indicates polymorphs that do not form dimers. For clarity electrostatic interactions between layers have been removed.

interactions. The dipolar moment is a measure of the separation of positive and negative charges within a molecule or crystal, and a larger dipolar moment indicates a greater degree of polarity. Hence, the lowest values of dipole moment are observed for polymorphs V, VI and IV, respectively, indicating therefore that the electrostatic intermolecular interactions don't play a fundamental role in the stability of these polymorphs. However, these interactions provide significant contributions in the other four polymorphs, and in particular, in the new polymorph (GAM-VII) which is characterised by the largest dipole moment. Therefore, this suggests that GAM-VII exhibits the strongest polar interactions among the other polymorphs, such as dipole–dipole interactions and potential hydrogen bonding. These stronger interactions can significantly influence the material's physical properties, such as melting point, solubility, and stability.

This interesting finding is consistent with the experimental structural investigation results. Indeed, the presence of disordered water molecules in the crystal structure of GAM-VII can contribute to an increase in the overall dipolar moment of the crystal. This is because water molecules are highly polar due to their bent molecular structure and the significant electronegativity difference

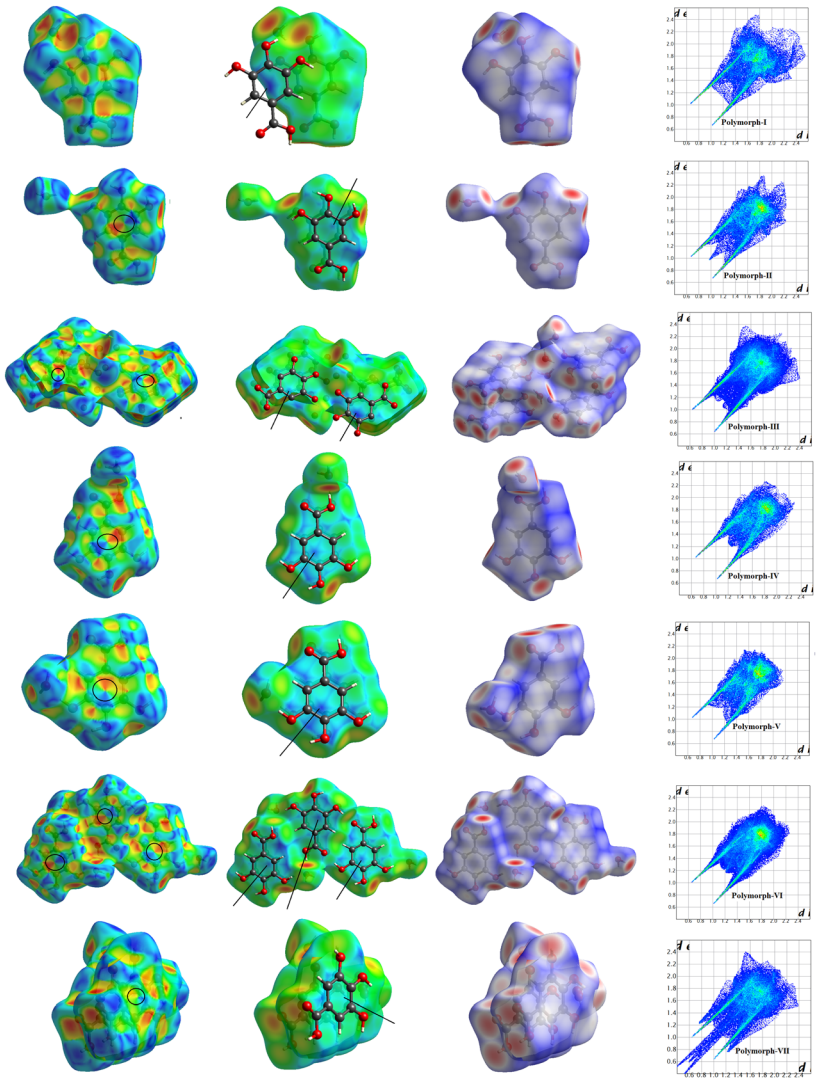

Fig. 5 Hirshfeld surfaces and 2D fingerprint plots for the seven polymorphs of GAM. From left to right, for each polymorph the Hirshfeld surface is shown mapped with shape index, d_e, d_{norm}, and fingerprint plots.

Table 3 Relative energy and global electronic density descriptors of gallic acid structures in eV

Geometry		Relative energy (eV)	Dipolar moment (Debye)	Vertical ionisation energy (eV)	Vertical electron affinity (eV)	Chemical hardness (eV)	Chemical softness (eV)	Chemical potential (eV)	Electronegativity (eV)	Electrophilicity (eV)
Polymorph-I		3.1988	3.2818	9.1874	−0.7004	4.9439	0.1011	−4.2435	4.2435	1.8212
Polymorph-II		2.0630	1.6684	9.0422	−0.7652	4.9037	0.1020	−4.1385	4.1385	1.7464
Polymorph-III	Mol 1	1.3538	3.3015	8.7784	−0.6917	4.7351	0.1056	−4.0433	4.0433	1.6918
	Mol 2	1.3262	3.6309	8.9813	−0.6822	4.8317	0.1035	−4.1495	4.1495	1.7818
	Mol 3	1.4895	4.7946	9.0732	−0.6596	4.8664	0.1027	−4.2068	4.2068	1.8183
	Mol 4	1.3510	4.8782	9.0003	−0.6487	4.8245	0.1036	−4.1758	4.1758	1.8072
Polymorph-IV		0.0621	1.1001	8.9927	−0.7861	4.8894	0.1023	−4.1033	4.1033	1.7278
Polymorph-V		0.0000	0.6222	8.7826	−0.7810	4.7836	0.1045	−4.0008	4.0008	1.6731
Polymorph-VI	Mol 1	2.0094	0.9966	8.9149	−0.7921	4.8535	0.1030	−4.0614	4.0614	1.7019
	Mol 2	1.6780	0.9767	8.9301	−0.7937	4.8619	0.1028	−4.0682	4.0682	1.6964
	Mol 3	1.8541	0.9199	8.9268	−0.7918	4.8593	0.1029	−4.0675	4.0675	1.7024
Polymorph-VII	Mol 1	2.5612	4.9946	8.8792	−0.6920	4.7 856	0.1045	−4.0936	4.0936	1.7508
	Mol 2	4.6361	5.1646	8.9858	−0.7009	4.8434	0.10 323	−4.14245	4.14245	1.7715

between oxygen and hydrogen atoms. Moreover, disordered water molecules participate more in polar interactions with neighbouring molecules through hydrogen bonding (Table 2) and dipole–dipole interactions. These additional interactions contribute to an increase in the overall dipolar moment of the crystal. Further, we have shown that the contributions of water molecules in the network of intermolecular interactions for GAM-VII are very strong and more particularly the disordered O2W molecule plays a unique role by being a triple donor and double acceptor of hydrogen bonds thus leading to the strengthening of electrostatic interactions in this new polymorph.

On the other hand, the Hirshfeld surface analyses based on experimental structural determination show that electrostatic interactions in GAM-VII have an important contribution to the HS. Electrostatic interactions refer to the attractive or repulsive forces between charged particles, such as ions or polar molecules. These interactions influence the spatial arrangement and stability of the crystal structure.

Electronegativity is a measure of an atom's ability to attract electrons in a chemical bond. This means how strongly the atoms in GA attract electrons towards themselves. The GA electronegativity shows weak sensitivity to stacking changes. The most electronegative GA structure is polymorph-I. This means that GA molecules in polymorph-I have a relatively stronger tendency to attract electrons compared to the other polymorphs.

Minimal differences are noted between chemical potential values, indicating that all GA structures have the same tendency of charge transfer from higher potential to lower potential regions. As hardness results show, GA is more resistant to using electrons in the polymorph-I structure. The softness of GA has slightly the same values for all structures. Fig. 6 shows that the HOMO–LUMO gap is maximum for GA in the polymorph-I structure. The low HOMO–LUMO is obtained for one GA molecule in polymorph-III.

The HOMO is a π molecular orbital type delocalized on all carbon and oxygen atoms in all structures. It is a result of both bonding and antibonding of carbon and oxygen π atomic orbitals. Meanwhile the LUMO is the antibonding molecular orbital localized on one hydroxyl group. This indicates that the hydroxyl group is the most reactive.

Conclusion

In order to adapt the physico-chemical properties of an active pharmaceutical ingredient (API), the way often chosen consists in exploring its solid forms, including polymorphs. Indeed, this work presents the synthesis, crystal structure, and theoretical study of the seventh pharmaceutical polymorph of gallic acid monohydrate (GAM-VII). The results highlight the significance of exploring new APIs for the advancement of the pharmaceutical industry. The findings shed light on the role of water molecules as design elements in crystal engineering, facilitating the formation and stability of this new polymorph through moderate intermolecular interactions involving carboxyl groups. In fact, in GAM-VII the disordered water molecule O2W plays a quintuple role and greatly contributes to the strengthening of electrostatic interactions in this new polymorph. This unique role has not been observed in any other GAM polymorph. Furthermore, the stacking of GA molecules is stabilized in the crystal packing of GAM-VII by water bridges; this effect should be considered as important in crystal engineering. The presence of a disordered water molecule in the crystal structure of GAM-VII adds an intriguing dimension to the study, and its role in the intermolecular interactions contributes to the unique properties and stability of this new polymorph.

GA molecules in GAM-VII adopt a *syn* COOH conformation and form the most common acid dimer synthon $R_2^2(8)$, which was previously observed only in a subset of GAM polymorphs. Further, GA molecules have three OH groups and their

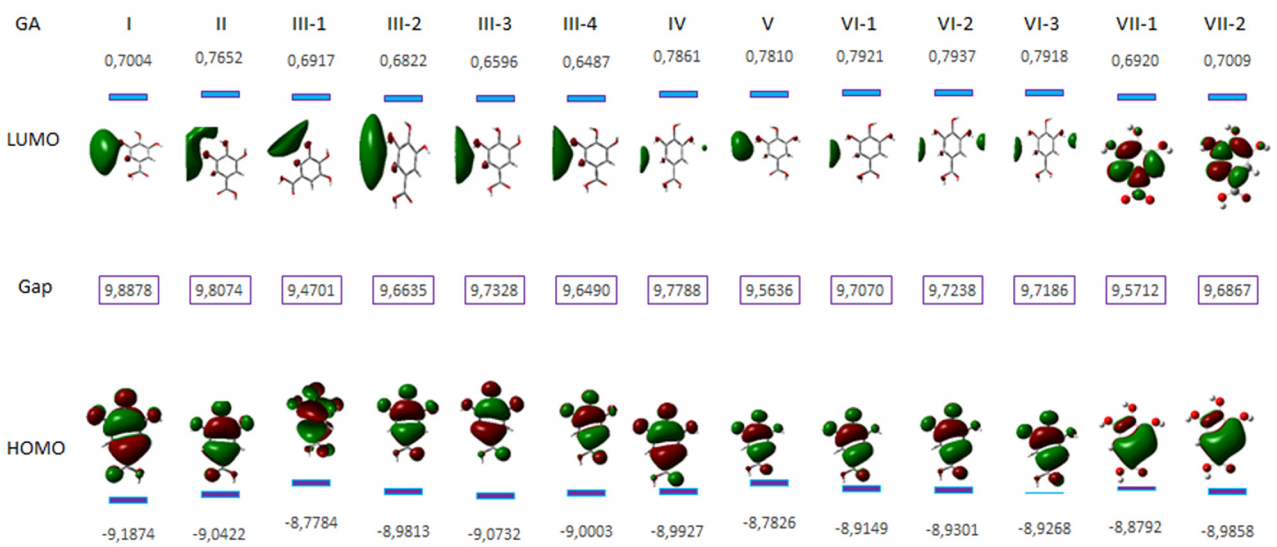

Fig. 6 HOMO and LUMO of the seven GAM polymorphs. Energies and electronic densities are in eV.

orientations shift under the effect of the interactions with the water molecule and with other Ga molecules. The crystal structure is primarily stabilized by strong O–H···O hydrogen bonds and aromatic stacking interactions. In the structures of the seven polymorphs, extended strong O–H···O interactions dictate the packing motifs.

The investigation of intermolecular interactions using fingerprint plots and a Hirshfeld surface (HS) method provide a deeper understanding of the offset stacking arrangement of GA molecules and the presence of π···π interactions between the benzene rings in all polymorphic structures except polymorph-I. Further, these analyses show that the main contributions to the Hirshfeld surfaces areas are provided by O···H interactions.

Complementary theoretical calculations offer valuable insights into the reactivity process of this new polymorph, including dipole moment, ionization and chemical potential, electronegativity, and electrophilicity index. These results demonstrate the distinctive properties of GAM-VII, indicating stronger polar interactions and enhanced stability due to the presence of disordered water molecules.

The research presented in this article sheds light on the rich polymorphism of gallic acid monohydrate and underscores the importance of water molecules as design elements in crystal engineering. Moreover, this work showcases the significance of polymorphism in APIs and emphasizes the potential impact of exploring new polymorphs on pharmaceutical processability, bioavailability, and medication stability. The detailed analysis of molecular conformations, hydrogen bonding patterns, and intermolecular interactions can inspire the design of new drug formulations and improve drug delivery methods. Moreover, the use of computational quantum chemistry approaches highlights the importance of understanding electronic density descriptors for predicting the stability and properties of different polymorphs.

Conflicts of interest

There are no conflicts of interest to declare.

Acknowledgements

We gratefully acknowledge the X-ray diffraction platform PMD^{2}X of the Université de Lorraine for providing access to the X-ray diffraction facilities. We also thank the Algerian MESRS (Ministère de l'Enseignement Supérieur et de la Recherche Scientifique) and DGRSDT (Direction Générale de la Recherche Scientifique et du Développement Technologique) and Abbes Laghrour Khenchela University for financial support.

References

1 M. R. Caira, Crystalline Polymorphism of Organic Compounds, *Design of Organic Solids*, Springer, Berlin, Heidelberg, 1998, vol. 198, pp. 163–208.
2 J. Bernstein, R. J. Davey and J. O. Henck, *Angew. Chem., Int. Ed.*, 1999, **38**, 3440–3460.
3 H. G. Brittain, in *Polymorphism in Pharmaceutical Solids*, Marcel Dekker, New York, 2nd edn, 1999.
4 J. Bernstein, *Polymorphism in Molecular Crystals*, Oxford University Press, Oxford, 2002.
5 N. Blagden and R. Davey, *Cryst. Growth Des.*, 2003, **3**, 873–885.
6 P. H. Karpinski, *Chem. Eng. Technol.*, 2006, **29**(2), 233–237.
7 H. G. Brittain, *Polymorphism in Pharmaceutical Solids*, CRC Press, Boca Raton, 2009.
8 S. R. Vippagunta, H. G. Brittain and D. J. W. Grant, *Adv. Drug Delivery Rev.*, 2001, **48**, 3–26.
9 S. Varughese and G. R. Desiraju, *Cryst. Growth Des.*, 2010, **10**, 4184–4196.
10 R. K. Khankari and D. J. W. Grant, *Thermochim. Acta*, 1995, **248**, 61–79.
11 H. P. Stahl, *Towards Better Safety of Drugs and Pharmaceutical Products. by DD. Braimar*, Elsevier/North-Holland Biomedical Press, Amsterdam, 1980, pp. 265–280.
12 C. R. Groom, I. J. Bruno, M. P. Lightfoot and S. C. Ward, *Acta Crystallogr., Sect. B: Struct. Sci., Cryst. Eng. Mater.*, 2016, **72**, 171–179.
13 A. L. Gillon, N. Feeder, R. J. Davey and R. Storey, *Cryst. Growth Des.*, 2003, **3**, 663–673.
14 M. B. Hickey, M. L. Peterson, E. S. Manas, J. Alvarez, F. Haeffner and Ö. Almarsson, *J. Pharm. Sci.*, 2007, **96**, 1090–1099.
15 X. Zhao, W. Zhang and S. Kong, *J. Liq. Chromatogr. Relat. Technol.*, 2007, **30**, 235–244.
16 B. Badhani, N. Sharma and R. Kakkar, *RSC Adv.*, 2015, **5**, 27540–27557.
17 Y. Liu, T. L. Pukala, I. F. Musgrave, D. M. Williams, F. C. Dehle and J. A. Carver, *Bioorg. Med. Chem. Lett.*, 2013, **23**, 6336–6340.
18 S. M. Fiuza, C. Gomes, L. J. Teixeira, M. T. Girão da Cruz, M. N. D. S. Cordeiro, N. Milhazes, F. Borges and M. P. M. Marques, *Bioorg. Med. Chem.*, 2004, **12**, 3581–3589.
19 S. Choubey, L. R. Varughese, V. Kumar and V. Beniwal, *Pharm. Pat. Anal.*, 2015, **4**, 305–315.
20 N. Hirun, S. Dokmaisrijan and V. Tantishaiyakul, *Spectrochim. Acta, Part A*, 2012, **86**, 93–100.
21 R. Kaur, S. Cherukuvada, P. B. Managutti and T. N. Guru Row, *CrystEngComm*, 2016, **18**, 3191.
22 R.-W. Jiang, D.-S. Ming, P. P. H. But and T. C. W. Mak, *Acta Crystallogr., Sect. C: Cryst. Struct. Commun.*, 2000, **56**, 594–595.
23 N. Okabe, H. Kyoyama and M. Suzuki, *Acta Crystallogr., Sect. E: Struct. Rep. Online*, 2001, **57**, o764–o766.
24 H. D. Clarke, K. K. Arora, Ł. Wojtas and M. J. Zaworotko, *Cryst. Growth Des.*, 2011, **11**, 964–966.
25 G. Demirtas, N. Dege and O. Büyükgüngör, *Acta Crystallogr., Sect. E: Struct. Rep. Online*, 2011, **67**, o1509–o1510.
26 D. E. Braun, R. M. Bhardwaj, A. J. Florence, D. A. Tocher and S. L. Price, *Cryst. Growth Des.*, 2013, **13**, 19–23.
27 A. A. Hoser, I. Sovago, A. Lanzac and A. Ø. Madsen, *Chem. Commun.*, 2017, **53**, 925–928.
28 J. Zhao, I. A. Khan and F. R. Fronczek, *Acta Crystallogr., Sect. E: Struct. Rep. Online*, 2011, **67**, o316–o317.

29 R. Benali-Cherif, R. Takouachet, W. Falek, N. Benali-Cherif, C. Jelsch, H. Merazig, M. Hafied, E.-E. Bendeif, N. B. Mokhnachi and K. Taibi, *J. Mol. Struct.*, 2021, **1224**, 129034.
30 R. Takouachet, R. Benali-Cherif, E.-E. Bendeif, N. Benali-Cherif, S. Pillet and D. Schaniel, *Inorg. Chim. Acta*, 2016, **446**, 6–12.
31 R. Benali-Cherif, R. Takouachet, E.-E. Bendeif and N. Benali-Cherif, *Acta Crystallogr., Sect. C: Struct. Chem.*, 2014, **70**, 689–692.
32 R. Benali-Cherif, R. Takouachet, E.-E. Bendeif and N. Benali-Cherif, *Acta Crystallogr., Sect. C: Struct. Chem.*, 2014, **70**, 323–325.
33 V. K. Rajan and K. Muraleedharan, *Food Chem.*, 2017, **220**, 93–99.
34 M. C. Burla, R. Caliandro, B. Carrozzini, G. L. Cascarano, C. Cuocci, C. Giacovazzo, M. Mallamo, A. Mazzone and G. Polidori, *J. Appl. Crystallogr.*, 2015, **48**, 306–309.
35 G. M. Sheldrick, *Acta Crystallogr., Sect. C: Struct. Chem.*, 2015, **71**, 3–8.
36 L. J. Farrugia, *J. Appl. Crystallogr.*, 2012, **45**, 849–854.
37 C. F. Macrae, I. J. Bruno, J. A. Chisholm, P. R. Edgington, P. McCabe, E. Pidcock, L. Rodriguez-Monge, R. Taylor, J. van de Streek and P. A. Wood, *J. Appl. Crystallogr.*, 2008, **41**, 466–470.
38 M. J. Frisch, G. W. Trucks, H. B. Schlegel, G. E. Scuseria, M. A. Robb, J. R. Cheeseman, G. Scalmani, V. Barone, G. A. Petersson, H. Nakatsuji, X. Li, M. Caricato, A. Marenich, J. Bloino, B. G. Janesko, R. Gomperts, B. Mennucci, H. P. Hratchian, J. V. Ortiz, A. F. Izmaylov, J. L. Sonnenberg, D. Williams-Young, F. Ding, F. Lipparini, F. Egidi, J. Goings, B. Peng, A. Petrone, T. Henderson, D. Ranasinghe, V. G. Zakrzewski, J. Gao, N. Rega, G. Zheng, W. Liang, M. Hada, M. Ehara, K. Toyota, R. Fukuda, J. Hasegawa, M. Ishida, T. Nakajima, Y. Honda, O. Kitao, H. Nakai, T. Vreven, K. Throssell, J. A. Montgomery Jr. , J. E. Peralta, F. Ogliaro, M. Bearpark, J. J. Heyd, E. Brothers, K. N. Kudin, V. N. Staroverov, T. Keith, R. Kobayashi, J. Normand, K. Raghavachari, A. Rendell, J. C. Burant, S. S. Iyengar, J. Tomasi, M. Cossi, J. M. Millam, M. Klene, C. Adamo, R. Cammi, J. W. Ochterski, R. L. Martin, K. Morokuma, O. Farkas, J. B. Foresman and D. J. Fox, *Gaussian 09, Revision A.02*, Gaussian, Inc., Wallingford CT, 2016.
39 J. Bernstein, R. E. Davis, L. Shimoni and N.-L. Chang, *Angew. Chem., Int. Ed. Engl.*, 1995, **34**, 1555–1573.
40 M. A. Spackman and D. Jayatilaka, *CrystEngComm*, 2009, **11**, 19–32.

